International Journal of Design & Nature and Ecodynamics
Vol. 21, No. 7, July, 2026, pp. 2133-2141
Journal homepage: http://iieta.org/journals/ijdne

Green Synthesis of Cobalt Oxide Nanoparticles Using the Freshwater Alga *Spirogyra* sp. and Evaluation of Their in Vitro Antifungal Activity

Maarb Salih Al-Maoula*, Noor Redha Gummaa, Ahmed S. Dwaish, Adel Hamdan Alwan, Rand Haider Ali, Estabraq Mohammed Ati

Department of Biology, College of Science, Mustansiriyah University, Baghdad 10052, Iraq

Corresponding Author Email: maarb.salih_abd@uomustansiriyah.edu.iq

https://doi.org/10.18280/ijdne.210725

Received: 17 May 2026
Revised: 9 July 2026
Accepted: 16 July 2026
Available online: 31 July 2026

Keywords:
biosynthesized cobalt oxide nanoparticles, freshwater alga

ABSTRACT

This study aimed to develop a green and sustainable method for synthesizing cobalt oxide nanoparticles using an ethanolic extract of the freshwater alga *Spirogyra* sp., and to evaluate their antifungal efficacy. Gas Chromatography–Mass Spectrometry (GC–MS) analysis of the algal ethanolic extract enabled the tentative identification of volatile and semi-volatile compounds that may be associated with algal metabolites. The synthesized cobalt oxide nanoparticles were characterized using UV–Vis spectroscopy, X-ray diffraction (XRD), and Scanning Electron Microscopy (SEM) imaging. Finally, the comparative antifungal activity of both the crude extract and the nanoparticles was evaluated against the pathogenic fungi *Fusarium* spp., *Curvularia* sp., and *Rhizoctonia* sp. The characterization results suggested the formation of crystalline cobalt oxide nanoparticles. While the crude algal extract showed limited antifungal activity, the biosynthesized nanoparticles demonstrated a substantial increase in inhibitory effects, achieving near-complete inhibition against most tested fungi at higher concentrations, possibly due to their increased surface reactivity and physicochemical properties. *Spirogyra* sp. represents a promising biological resource for the green synthesis of cobalt oxide nanoparticles. The present findings demonstrate the potential of the biosynthesized nanoparticles for in vitro antifungal applications. However, further studies are required to confirm the crystal phase, evaluate their safety, stability, and reproducibility, and assess their suitability for practical biomedical and agricultural applications.

1. INTRODUCTION

Nanotechnology is revolutionizing biomedical research through the facilitation of the synthesis of new materials with special properties, particularly metal and metal oxide nanoparticles with high antimicrobial potential. Cobalt oxide (CoO/Co_3O_4) nanoparticles are gaining attention because of their unique physicochemical properties and potential biomedical, agricultural, catalytic, and antimicrobial applications [1]. Traditional synthesis methods often use poisonous chemicals and energy-intensive processes, raising concerns regarding environmental safety and sustainability. To overcome these challenges, green synthesis methods have emerged as attractive alternatives. These approaches employ natural biological agents such as plant extracts, fungi, and algae to reduce metal salts into nanoparticles [2]. Algae, especially freshwater species such as *Spirogyra*, are rich in metabolites including polyphenols, proteins, and flavonoids that can act as both reducing and capping agents during nanoparticle synthesis [3]. Phenolic compounds and flavonoids can donate electrons during nanoparticle formation, while proteins and polysaccharides contribute to nanoparticle stabilization and prevention of aggregation. Their abundance, renewability, and rich biochemical composition make them suitable candidates for the sustainable production of nanomaterials. The filamentous green alga *Spirogyra* sp. is widespread in freshwater habitats and has shown potential for the biosynthesis of metallic nanoparticles. The presence of diverse bioactive metabolites, including phenolic compounds, proteins, flavonoids, and polysaccharides, makes *Spirogyra* sp. a promising biological resource for nanoparticle synthesis [4]. Furthermore, cobalt oxide nanoparticles possess high surface area, catalytic activity, and the ability to induce reactive oxygen species (ROS), which contribute to their antimicrobial properties. However, the effectiveness of antimicrobial agents may vary depending on the intrinsic biological characteristics, genetic background, and adaptive mechanisms of microbial organisms. Previous studies on bacterial pathogens have demonstrated that genetic determinants associated with virulence, adhesion, and resistance profiles can influence microbial survival and response to antimicrobial stress [5, 6].

Although numerous studies have reported the green synthesis of metallic and metal oxide nanoparticles using plant and algal extracts, only limited studies have investigated the biosynthesis of cobalt oxide nanoparticles using the freshwater alga *Spirogyra* sp. Furthermore, information regarding the antifungal activity of biosynthesized cobalt oxide

nanoparticles produced from this algal species against phytopathogenic fungi remains limited. Therefore, the present study was designed to investigate the biosynthesis of cobalt oxide nanoparticles using *Spirogyra* sp. ethanolic extract and to evaluate their in vitro antifungal activity against selected phytopathogenic fungi. Unlike many previous studies focusing mainly on plant-mediated synthesis of metal oxide nanoparticles, this work explores *Spirogyra* sp. as a freshwater algal source for cobalt oxide nanoparticle synthesis and evaluates its antifungal potential against phytopathogenic fungi isolated from local agricultural environments. The novelty of this study lies in combining algal-mediated cobalt oxide synthesis with preliminary in vitro antifungal assessment.

2. MATERIAL AND METHOD

2.1 Collection and preparation of samples

Samples were collected from the Tigris River, Al-Rashidiya District, Baghdad, Iraq, during the winter of 2024. Freshwater algal samples were collected from areas showing abundant algal growth using sterile sampling equipment. Identification was performed using standard morphological and morphometric characteristics according to published taxonomic keys [7]. The sampling sites were chosen according to their easy access and dense algal mats, where the biomass was carefully collected by scraping it from rocks and submerged substrates using sterilized equipment. Field surveys were performed at different agricultural fields in Baghdad to collect infected roots, fruits, and rhizosphere soils from tomato, okra, and strawberry crops. For the plant samples, the collected materials were washed and surface-sterilized by soaking in 0.6% sodium hypochlorite solution for 2–3 min. Subsequently, the materials were rinsed twice with sterile distilled water and air-dried. The samples were then cut into small pieces and plated on Potato Dextrose Agar (PDA) supplemented with 50 µg/mL chloramphenicol. Similarly, fungi associated with rhizosphere soils were isolated using the conventional serial dilution plating method on the same medium. All plates were incubated at 28 ℃ for 3–6 days, after which pure fungal cultures were obtained by repeated subculturing. The isolated fungal cultures were maintained on PDA slants at 4 ℃ in the fungal culture collection of the Department of Biology, College of Science, Mustansiriyah University, Baghdad, Iraq, until further analyses. The fungal isolates used in the antifungal assay were identified based on colony morphology and microscopic characteristics, including mycelial growth pattern, colony color, and reproductive structures, according to standard fungal identification keys [7]. Since molecular identification was not performed, the identification was considered morphological. The fungal isolates used in the antifungal assay were characterized based on macroscopic colony morphology and microscopic characteristics according to standard fungal identification keys [7]. The morphological evaluation included colony appearance, pigmentation, growth pattern, mycelial characteristics, and reproductive structures, including hyphal features and conidial morphology when present. Based on these observations, the isolates were assigned as *Fusarium oxysporum*-like, *Fusarium solani*-like, *Fusarium subglutinans*-like, *Curvularia* sp., and *Rhizoctonia* sp. Since molecular identification using specific markers (e.g., Internal Transcribed Spacer (ITS), Elongation Factor 1-alpha (EF-1α), or β-tubulin sequencing) was not performed, the species-level identification of *Fusarium* isolates should be considered tentative and based on morphological similarity. Before antifungal evaluation, actively growing seven-day-old fungal cultures were used, and 5-mm mycelial discs were obtained from the actively growing margins of the colonies.

2.2 Extraction of algae using ethanolic Soxhlet extraction

The dried biomass of *Spirogyra* sp. was ground into a fine powder using a mechanical grinder. Approximately 50 grams of the powdered algal material were subjected to Soxhlet extraction using 95% ethanol as the solvent. The extraction was carried out continuously for 6 hours to ensure maximum recovery of secondary metabolites. The solvent was heated to reflux and cycled through the algal powder repeatedly, allowing efficient dissolution of bioactive compounds. After extraction, the ethanolic extract was concentrated under reduced pressure using a rotary evaporator at 40 ℃ to remove the solvent, yielding a crude concentrated extract. This extract was stored in amber-colored bottles at 4 ℃ until further phytochemical and biological analyses were performed. The crude extract was completely concentrated using a rotary evaporator to ensure the complete removal of residual ethanol before further analyses [8].

2.3 Green synthesis of nanoparticles using algae extract

Cobalt nitrate hexahydrate ($Co(NO_3)_2 \cdot 6H_2O$) was used as the cobalt precursor. A 0.2 M cobalt nitrate hexahydrate solution was prepared by dissolving 9.31 g in 160 mL of deionized water. Subsequently, 40 mL of the ethanolic extract of *Spirogyra* sp. was added to the precursor solution, and the mixture was stirred for 10 min. The resulting suspension was transferred into a glass autoclave and heated at 80 ℃ for 3 h using a laboratory furnace. After the reaction, the autoclave was allowed to cool naturally to room temperature. The obtained precipitate was washed three times with distilled water followed by absolute ethanol to remove residual impurities and unreacted precursor. The purified product was dried and then annealed at 300 ℃ for 1 h to remove residual organic compounds. Finally, the synthesized cobalt oxide nanoparticles were stored in sealed amber glass containers at room temperature until further characterization and biological evaluation.

2.4 Characterization of synthesized nanoparticles

2.4.1 UV-Visible absorption spectroscopy

The optical absorption spectra of the nanoparticles were measured using UV spectroscopy. The nanoparticles were dispersed in deionized distilled water and subjected to ultrasonication for 15 minutes. For optical properties, the absorption factor, transmission tests, and band gap estimations have all been determined and published. The absorption rate of algae-generated nanoparticles was detected in the range of wavelengths 200-800 nm. Also, the energy band gap was calculated by the Tauc and Wood plot formula [9].

2.4.2 X-ray diffraction

X-ray diffraction (XRD) was used to identify the crystal structure (phases) as well as the size, organization, and physical characteristics of nanoparticles. Diffraction peaks of the samples were identified by comparison with the "Joint

Committee on Powder Diffraction (JCPDS) Standards". The full width at half maximum (FWHM) of the XRD peaks was used to calculate the crystallite size using Scherrer's formula [10, 11].

2.4.3 Scanning Electron Microscope

The samples were prepared using standard protocols, which included spreading them over the surface of a glass slide. The nanoparticle sample was subsequently made available for examination [12, 13].

2.5 Antifungal activity assay

The antifungal activity of the *Spirogyra* sp. ethanolic extract and biosynthesized cobalt oxide nanoparticles was evaluated using the poisoned food technique on PDA. The crude algal extract and Co_3O_4 nanoparticle suspensions were incorporated into molten PDA medium before solidification. Briefly, PDA medium was sterilized by autoclaving and allowed to cool to approximately 45 °C before the addition of the tested materials to avoid thermal degradation of bioactive compounds.

Stock solutions of the algal extract were prepared at concentrations of 50, 100, and 200 mg/mL. These concentrations represented the stock solutions and were diluted after incorporation into PDA medium to obtain final exposure concentrations of 2500, 5000, and 10000 µg/mL, respectively. For nanoparticle treatments, the synthesized cobalt oxide nanoparticles were dispersed in sterile distilled water and sonicated for 15 min to obtain a uniform suspension before incorporation into PDA. A volume of 1 mL of each stock solution or nanoparticle suspension was added to 19 mL of molten PDA medium to obtain final concentrations of 2500, 5000, and 10000 µg/mL, respectively, with a final volume of 20 mL per Petri dish.

The pH of the PDA medium was adjusted to 5.5 before inoculation with fungal cultures. Control treatments were included to evaluate the possible antifungal effects of residual components associated with the extraction and nanoparticle synthesis procedures. Untreated PDA plates were used as negative controls. An ethanol control containing the same volume of ethanol used during extract preparation was included to assess any inhibitory effect caused by residual solvent. A cobalt nitrate precursor control was included to determine whether cobalt ions originating from the synthesis precursor could contribute to the observed antifungal activity. The cobalt nitrate hexahydrate solution was prepared and tested under the same antifungal assay conditions to allow comparison between the precursor salt and the synthesized cobalt oxide nanoparticles. A blank preparation control was also included to exclude any antifungal activity resulting from the nanoparticle preparation process itself. After solidification, a 5-mm diameter mycelial disc taken from the actively growing margin of seven-day-old fungal cultures was placed at the center of each treated plate. All treatments were performed in triplicate and incubated at 25 °C in darkness for seven days. Colony diameter was measured, and percentage inhibition of fungal growth was calculated using the following equation:

$$Inhibition\ (\%) = \frac{C - T}{C} \times 100\%$$

where, C represents the colony diameter of the control plate, and T represents the colony diameter of the treated plate [14].

2.6 Statistical analysis

All experiments were performed in triplicate (n = 3). The results are expressed as mean ± standard deviation (SD). Statistical analysis was performed using two-way analysis of variance (Two-way ANOVA) to evaluate the effect of treatment type and concentration on antifungal activity. Post-hoc comparisons between group means were conducted using Tukey's Honestly Significant Difference (HSD) test. Statistical significance was considered at $p < 0.05$.

3. RESULTS

3.1 Morphological characteristics and taxonomic

Microscopic analysis of the freshwater samples collected from Al-Rashidiya region, Baghdad, Iraq, during winter 2024 revealed the presence of unbranched filamentous green algae. The isolate was morphologically identified as *Spirogyra* sp. based on its characteristic vegetative features. Vegetative cells were cylindrical with plane transverse end walls and measured 26.0–28.0 µm in diameter, with a mean value of 27.1 ± 0.7 µm (n = 50). Cell length showed a wider range, varying from 148.0 to 350.0 µm, with an average of 248.5 ± 62.3 µm. Each cell contained a single parietal, ribbon-shaped chloroplast arranged in a spiral form. The number of spiral turns per cell ranged between 0.5 and 3.0 complete turns (Figure 1).

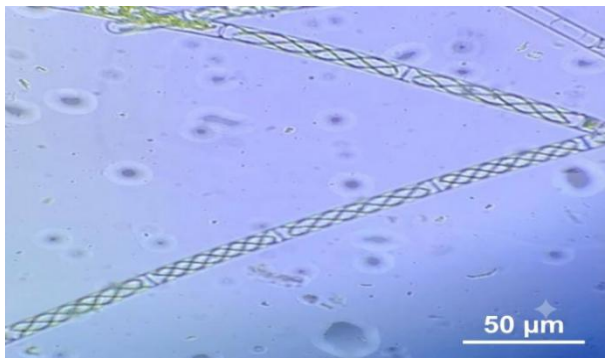

Figure 1. Light micrograph (40×) of *Spirogyra* sp. filaments collected from Al-Rashidiya showing the characteristic spiral chloroplast within cylindrical cells
Note: Scale bar: 50 µm.

During examination, cells located near fragmented ends of filaments were excluded from measurements because of their irregular dimensions. A comparative analysis of the recorded dimensions with previously published taxonomic data indicated a high degree of similarity. The morphological parameters of the Al-Rashidiya isolate fell within the ranges described for *Spirogyra* species by research [15] and were particularly close to those reported by research [16] for specimens collected from other Iraqi freshwater habitats. Based on morphological characteristics alone, the isolate was assigned to the genus *Spirogyra*. Species-level identification was not confirmed because molecular taxonomic analyses were not performed.

3.2 Morphological characterization of fungal isolates

The fungal isolates recovered from infected plant tissues and rhizosphere soils were characterized based on

macroscopic colony morphology and microscopic observations. Fusarium-like isolates exhibited typical filamentous growth with cottony colonies and variable pigmentation among isolates. Microscopic examination revealed hyaline septate hyphae and characteristic conidial structures consistent with the genus *Fusarium*. The *Curvularia* sp. isolate was distinguished by darkly pigmented colonies and curved, multicellular conidia, whereas the *Rhizoctonia* sp. isolate showed rapid mycelial growth with characteristic hyphal morphology and absence of conidial production under the tested conditions. Based on these morphological characteristics, the isolates were tentatively designated as *Fusarium oxysporum*-like, *Fusarium solani*-like, *Fusarium subglutinans*-like, *Curvularia* sp., and *Rhizoctonia* sp. Since molecular confirmation was not performed, these identifications represent morphological assignments and should be considered tentative rather than definitive species-level identifications. Representative colony morphology and microscopic features of the fungal isolates are presented in Figure 2.

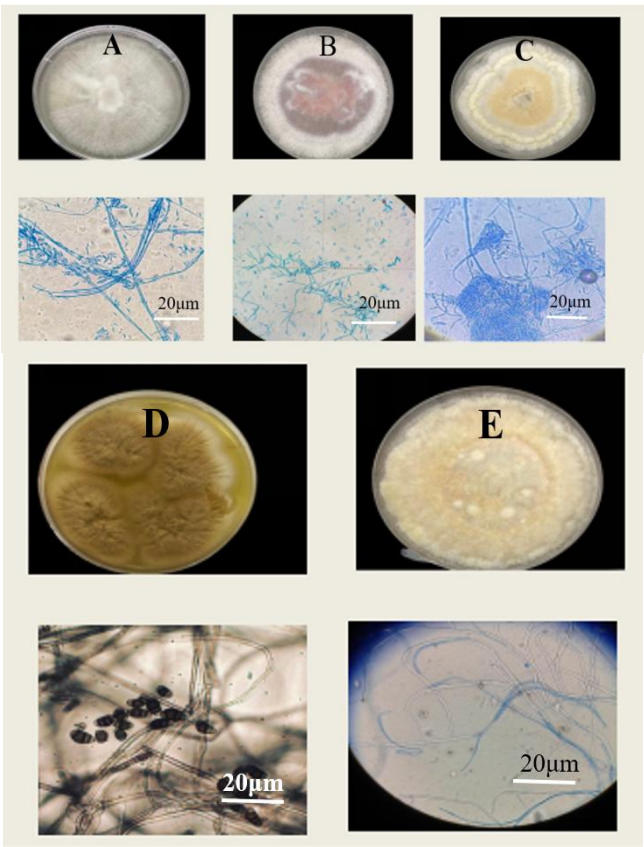

Figure 2. Macroscopic and microscopic characterization of fungal isolates recovered from infected plant tissues and rhizosphere soils. Representative fungal isolates grown on Potato Dextrose Agar (PDA) medium showing colony morphology and microscopic characteristics. (A) *Fusarium oxysporum*-like isolate, (B) *Fusarium solani*-like isolate, (C) *Fusarium subglutinans*-like isolate, (D) *Curvularia* sp. isolate, and (E) *Rhizoctonia* sp. isolate
Note: Microscopic observations were performed using light microscopy to evaluate characteristic fungal structures. Scale bars: 20 µm.

3.3 Gas Chromatography–Mass Spectrometry analysis of *Spirogyra* sp. ethanolic extract

Gas Chromatography–Mass Spectrometry (GC–MS) analysis of the ethanolic extract of *Spirogyra* sp. detected 18 integrated chromatographic peaks, as illustrated in the total ion chromatogram (TIC) (Figure 3). The investigated *Spirogyra* sp. represents a freshwater filamentous alga that has been previously reported in Iraqi aquatic environments, including the Tigris River, where different algal species were characterized based on morphological and taxonomic features [17]. The detected compounds were tentatively identified through comparison of their mass spectra with the W10N14.L mass-spectral library using library-matching criteria. To limit uncertain assignments, only first-ranked library matches with quality scores of ≥70% were retained for compound-level reporting in Table 1. Peaks with lower match-quality scores were classified as unidentified signals and excluded from the identification table. The five retained peaks accounted for 35.36% of the total integrated chromatographic peak area. Compound assignments were based on library matching and should therefore be regarded as tentative until confirmed using authentic standards and experimental retention indices.

The retained peaks were tentatively assigned to eucalyptol, 2-carene, (E)-hexadec-2-enal, neophytadiene, and 5,5'-diacetyl-3,3'-biisoxazole. Among these compounds, 2-carene accounted for 8.27% of the total integrated area, followed by eucalyptol at 8.03%, neophytadiene at 7.84%, the biisoxazole-related ethanone derivative at 6.58%, and (E)-hexadec-2-enal at 4.64%. Their library-match quality scores ranged from 72% to 99%. Previous investigations on *Spirogyra* extracts have demonstrated the presence of diverse bioactive metabolites, and GC–MS analysis has been used to characterize chemical constituents associated with potential biological activities in freshwater microalgae [18]. Nevertheless, these assignments remain tentative because they were based on spectral-library comparison without confirmation using authentic standards or experimental retention indices.

The largest integrated chromatographic peak occurred at 60.395 min and accounted for 47.14% of the total peak area. Its highest library-match quality was only 43%; therefore, it was classified as an unidentified major peak rather than assigned an uncertain chemical identity. A further peak at 61.352 min, accounting for 4.91% of the total area, showed a low-quality match to hexadecamethyloctasiloxane (50%). This signal was excluded from Table 1 because its low match quality precluded reliable identification and because siloxane signals may arise from column bleeding, septum components, or silicone-containing laboratory materials.

The detected compounds represent a preliminary chemical profile of the volatile and semi-volatile constituents present in the *Spirogyra* sp. ethanolic extract. Applying the ≥70% quality threshold reduced the risk of reporting uncertain compound identities but left signals representing 64.64% of the total integrated chromatographic area without reliable assignments. Therefore, the compounds listed in Table 1 should not be interpreted as a complete chemical profile of the extract.

Although some detected compounds have been reported in other biological systems, their contribution to cobalt oxide nanoparticle synthesis, stabilization, or antifungal activity in the present study cannot be confirmed based solely on GC–MS analysis. The detected compounds should therefore not be considered direct evidence of the biomolecules responsible for cobalt ion reduction, nanoparticle stabilization, or antifungal effects. Important biomolecules potentially involved in green nanoparticle synthesis, including phenolic compounds, flavonoids, proteins, and polysaccharides, may be non-volatile or thermally labile and may therefore not be adequately

detected by GC–MS. Determining their possible contribution requires complementary characterization using Fourier-transform infrared spectroscopy (FTIR), liquid chromatography–mass spectrometry (LC–MS), targeted phytochemical assays, or compound isolation followed by structural confirmation [19, 20].

Table 1. Tentatively identified volatile and semi-volatile compounds in the ethanolic extract of *Spirogyra* sp. based on first-ranked Gas Chromatography–Mass Spectrometry (GC–MS) library matches with quality scores of ≥70%

Peak No.	RT (min)	Area (%)	Tentatively Identified Compound	Quality (%)
1	18.229	8.03	Eucalyptol (1,8-cineole; 1,3,3-trimethyl-2-oxabicyclo[2.2.2]octane)	99
2	33.328	8.27	2-Carene	93
3	34.177	4.64	(E)-Hexadec-2-enal	90
11	52.484	7.84	Neophytadiene	98
13	53.989	6.58	5,5'-diacetyl-3,3'-biisoxazole	72
Total Identified Area		35.36		

Note: RT: Retention time. The analysis detected 18 integrated peaks in the *Spirogyra* sp. sample. The table includes only first-ranked library matches with quality scores of ≥70%. Peaks below this threshold were treated as unidentified and excluded from compound-level reporting. The listed compounds account for 35.36% of the total integrated chromatographic peak area. All assignments remain tentative until confirmed using authentic standards and experimental retention indices.

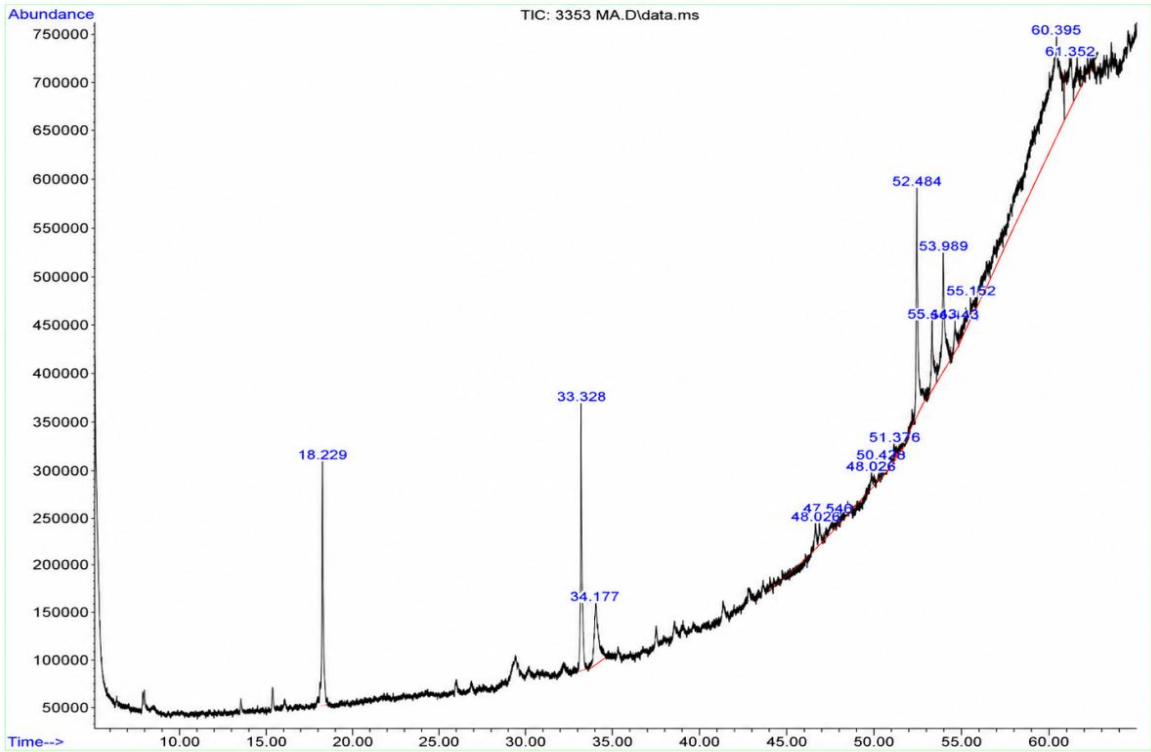

Figure 3. Gas Chromatography–Mass Spectrometry (GC–MS) total ion chromatogram of the ethanolic extract of *Spirogyra* sp. Tentatively identified peaks with library-match quality scores of ≥70% occurred at 18.229, 33.328, 34.177, 52.484, and 53.989 min. The largest integrated peak at 60.395 min remained unidentified because of its low library-match quality

3.4 Green synthesis of cobalt oxide nanoparticles

The main sources of biologically produced nanoparticles are microorganisms (such as bacteria, fungi, and yeast) and plant/algae synthesis [21-26]. Nanoparticles from algal and plant extracts are superior to those produced from microorganisms.

3.5 Characterization of green-synthesized nanoparticles

3.5.1 UV-Vis spectroscopic analysis

Optical absorption profile

The optical absorption characteristics of the prepared cobalt oxide nanoparticles (Co_3O_4) were analyzed using the UV-visible spectrophotometer technique in the wavelength region from 250 to 1100 nm, as shown in Figure 4(a). In the obtained absorption spectra, a strong UV absorption peak with a maximum value of 284 nm (0.643 Abs) and another peak around 515 nm (0.187 Abs) are found, which are typical signatures of the spinel (Co_3O_4) crystalline structure. The strong UV peak is due to the charge-transfer transition between oxygen and cobalt ions, whereas the secondary peak in the visible region is due to the d–d transition of cobalt ions [27, 28].

More importantly, the absence of a sharp Surface Plasmon Resonance (SPR) peak indicates that the prepared material contains metal oxide nanoparticles but not metal nanoparticles (e.g., copper and cobalt) [29, 30]. In addition, the biomolecules in *Spirogyra* sp. ethanolic extract, i.e., the natural molecules like phenols and flavonoids, effectively act as reducing and stabilizing agents in the green synthesis of these optically active cobalt oxide nanoparticles.

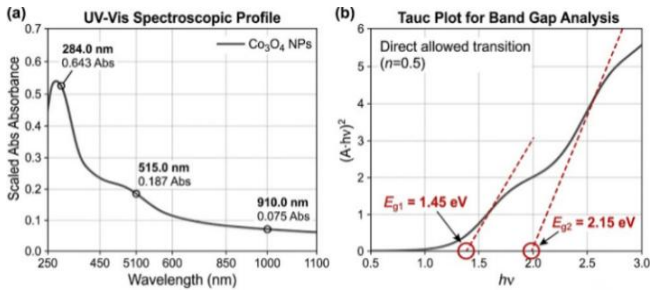

Figure 4. Comprehensive optical characterization of green-synthesized Co_3O_4 nanoparticles. (a) UV-Vis absorbance spectrum (250–1100 nm) showing distinctive features at 284.0 nm and 515.0 nm, (b) Tauc plot derived from (a) for direct allowed transitions, with E_{g1} and E_{g2} band gap energies determined by linear extrapolation to the photon energy axis (Y = 0)

Evaluation of optical band gap via Tauc plot

To evaluate the precise optical band gap energy (E_g) of the prepared sample, the Tauc relation for direct allowed electronic transitions (n = 1/2) was utilized, as expressed in Eq. (1):

$$(A.hv)^2 = B(hv - E_g) \quad (1)$$

where, *A* corresponds to the experimental absorbance, *hv* represents the incident photon energy (calculated via $hv = 1240/\lambda$), *B* is a material-dependent constant, and E_g is the optical band gap energy.

By plotting $(A.hv)^2$ against photon energy (hv), a Tauc plot was successfully constructed. Extrapolation of the linear segments of the curve to the photon energy axis (where $(A.hv)^2 = 0$) accurately determined the optical energy gaps. As illustrated in Figure 4(b), the sub-band gap (E_{g1}) was found to be 1.45 eV, whereas the fundamental main band gap (E_{g2}) was determined to be 2.15 eV.

Discussion of dual-band-gap behavior

The optical transition in Co_3O_4 is unique due to the simultaneous presence of Co^{2+} and Co^{3+} ions in tetrahedral and octahedral sites of the spinel lattice, respectively, which characteristically leads to this dual band gap behavior [31]. The first band gap (E_{g1} = 1.45 eV), observed at lower energy, is attributed to sub-bandgap transitions from the valence band to intermediate Co d-levels. The second, larger band gap (E_{g2} = 2.15 eV) represents the fundamental charge-transfer transition between the O 2p valence band and the Co^{3+} t_{2g} conduction band. To validate the reliability of these findings, the obtained values were compared with previous literature, showing excellent agreement with high-purity crystalline Co_3O_4 nanostructures synthesized via green routes [27, 31]. This agreement confirms that *Spirogyra* sp. extract successfully promoted the formation of optically active cobalt oxide nanoparticles.

3.5.2 X-ray diffraction analysis

The XRD pattern of the nanoparticles synthesized using *Spirogyra* sp. ethanolic extract showed diffraction peaks within the range of 2θ = 30–60° (Figure 5), indicating the formation of a crystalline cobalt oxide phase. Based on the available XRD data, the diffraction pattern is consistent with the formation of cobalt oxide nanoparticles; however, the precise crystal phase (CoO or Co_3O_4) cannot be conclusively assigned from the present results alone. Similar diffraction patterns have been reported for cobalt oxide nanomaterials synthesized by green methods, although distinguishing between CoO and Co_3O_4 requires complete peak indexing and comparison with standard reference data [29, 32]. The observed diffraction peaks are relatively broad and of low intensity, which is consistent with nanocrystalline cobalt oxide materials reported in previous studies [33]. This broadening may indicate relatively small crystallite size; however, crystallite size was not quantitatively estimated because Scherrer calculations were not performed.

Furthermore, the presence of background noise and irregular peak shapes suggests partial amorphous character and may be due to organic compounds from the *Spirogyra* sp. extract acting as capping and stabilizing agents. These biomolecules, such as phenolics and polysaccharides, can interfere with crystal growth, resulting in lower crystallinity and broader peaks [34]. Generally, the XRD results show that the synthesized material is composed of cobalt oxide nanoparticles prepared by a green synthesis with nanoscale size and moderate crystallinity using *Spirogyra* sp. extract.

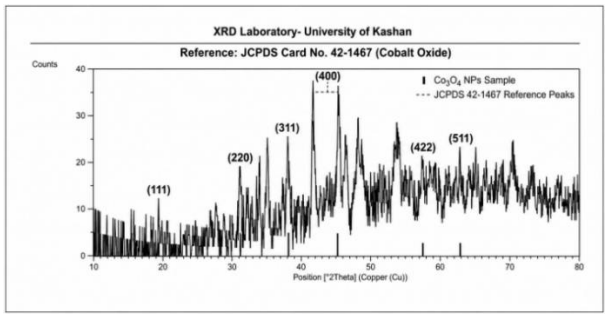

Figure 5. X-ray diffraction (XRD) pattern of cobalt oxide nanoparticles biosynthesized using *Spirogyra* sp. ethanolic extract

Note: The major diffraction peaks were indexed according to the Joint Committee on Powder Diffraction (JCPDS) reference card (No. 42-1467).

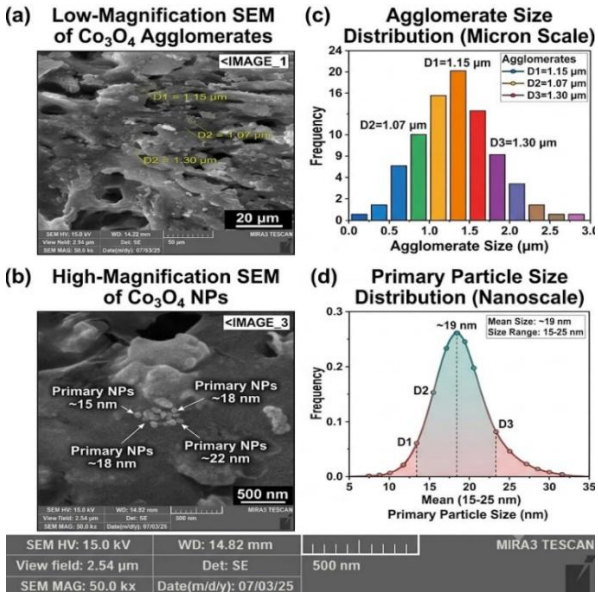

Figure 6. Scanning Electron Microscopy (SEM) morphology and size analysis of green-synthesized cobalt oxide material. (a) Low-magnification SEM image showing micron-scale aggregates, (b) high-magnification SEM image showing nanoscale primary particles forming the aggregates, (c) size distribution of aggregate structures with an average diameter of approximately 1.15 µm, (d) primary particle size distribution showing an average particle diameter of approximately 19 nm

3.5.3 Scanning Electron Microscopy

The Scanning Electron Microscopy (SEM) micrographs of the synthesized cobalt oxide material (Figure 6) revealed a highly clustered morphology with a rough and porous surface structure. The observed morphology indicates the presence of nanoscale primary particles forming larger micron-scale aggregates. The low-magnification SEM image (Figure 6(a)) showed aggregate structures ranging from approximately 1.07 to 1.30 µm. These micron-sized structures represent agglomerated assemblies of primary cobalt oxide particles rather than individual nanoparticles. Such aggregation is commonly observed in green-synthesized metal oxide materials due to high surface energy and interparticle interactions during drying and sample preparation [2, 4]. The high-magnification SEM image (Figure 6(b)) resolved these agglomerates into primary nanoscale particles within the aggregated structures, with representative particle diameters ranging from approximately 15 to 22 nm. The agglomerate-size distribution shown in Figure 6(c) indicated an average agglomerate diameter of approximately 1.15 µm, with measured values ranging from approximately 1.07 to 1.30 µm. Image-based particle-size analysis (Figure 6(d)) showed an overall primary particle size range of approximately 15–25 nm, with an average diameter of approximately 19 nm. These nanoscale primary particles were observed as aggregated clusters, indicating that the synthesized material exhibited both nanoscale primary particle dimensions and micron-scale aggregation behavior. Drying during SEM sample preparation may also contribute to particle agglomeration [35]. The observed morphology is consistent with the XRD results, which suggest the formation of a crystalline cobalt oxide nanostructured material. However, SEM does not provide direct information on crystal phase, and therefore phase identification was based on XRD analysis. Furthermore, the porous surface morphology may increase the effective surface area, which could be advantageous for catalytic and antimicrobial applications [36]. However, the presence of aggregation may influence nanoparticle dispersion, effective surface area, and biological interactions, and should be considered when interpreting the observed antimicrobial activity.

3.6 Antifungal activity of biosynthesized cobalt oxide nanoparticles

Antifungal activity of the ethanolic extract of *Spirogyra* sp. and its corresponding cobalt oxide nanoparticles was evaluated against selected fungal pathogens (Table 2). The crude *Spirogyra* sp. extract showed weak antifungal activity, with no inhibition (0%) against *Fusarium subglutinans*, *Curvularia* sp., and *Rhizoctonia* sp. at all tested concentrations, and only minimal inhibition against *Rhizoctonia* sp. at 10,000 µg/mL (17 ± 1.0%). Moderate inhibitory effects were observed against *Fusarium oxysporum* (85 ± 2.1% inhibition at 10000 µg/mL) and *Fusarium solani* (88 ± 1.8% inhibition at 10000 µg/mL), with reduced activity at lower concentrations. The biosynthesized CoO nanoparticles exhibited significantly enhanced antifungal activity compared with the crude algal extract. Complete inhibition (100%) was achieved against all tested fungal species at the highest concentration (10000 µg/mL). The inhibitory effect generally increased with increasing nanoparticle concentration, indicating a concentration-dependent antifungal response. For *Fusarium oxysporum*, *Curvularia* sp., and *Rhizoctonia* sp., complete inhibition (100%) was observed at all tested CoO nanoparticle concentrations (10000, 5000, and 2500 µg/mL). *Fusarium subglutinans* showed complete inhibition at 10000 and 5000 µg/mL, while 83 ± 1.5% inhibition was recorded at 2500 µg/mL. In contrast, *Fusarium solani* showed complete inhibition at 10000 and 5000 µg/mL, whereas inhibition decreased to 44 ± 2.0% at 2500 µg/mL.

The cobalt nitrate precursor control showed no detectable antifungal inhibition against the tested fungal isolates under the applied experimental conditions. This finding indicates that cobalt ions originating from the precursor salt alone were insufficient to inhibit fungal growth at the tested concentrations. Therefore, the enhanced antifungal activity observed for the synthesized cobalt oxide material may be related to the physicochemical characteristics of the nanoparticle form, including surface properties and particle–fungus interactions, rather than the presence of free cobalt ions alone.

Table 2. Antifungal activity of *Spirogyra* sp. ethanolic extract and biosynthesized cobalt oxide nanoparticles against selected fungal isolates

Fungal Isolate	Treatment	Growth Inhibition (%) at Each Concentration (µg/mL)		
		10,000	5,000	2,500
Fusarium subglutinans	Crude extract	0 ± 0.0^{c}	0 ± 0.0^{c}	0 ± 0.0^{c}
	Cobalt oxide nanoparticles	100 ± 0.0^{a}	100 ± 0.0^{a}	83 ± 1.5^{b}
Fusarium oxysporum	Crude extract	85 ± 2.1^{b}	0 ± 0.0^{c}	0 ± 0.0^{c}
	Cobalt oxide nanoparticles	100 ± 0.0^{a}	100 ± 0.0^{a}	100 ± 0.0^{a}
Fusarium solani	Crude extract	88 ± 1.8^{b}	31 ± 2.3^{c}	16 ± 1.2^{c}
	Cobalt oxide nanoparticles	100 ± 0.0^{a}	100 ± 0.0^{a}	44 ± 2.0^{b}
Curvularia sp.	Crude extract	0 ± 0.0^{c}	0 ± 0.0^{c}	0 ± 0.0^{c}
	Cobalt oxide nanoparticles	100 ± 0.0^{a}	100 ± 0.0^{a}	100 ± 0.0^{a}
Rhizoctonia sp.	Crude extract	17 ± 1.0^{c}	0 ± 0.0^{c}	0 ± 0.0^{c}
	Cobalt oxide nanoparticles	100 ± 0.0^{a}	100 ± 0.0^{a}	100 ± 0.0^{a}

Note: Data are presented as mean ± SD of three independent replicates (n = 3). Within each fungal isolate, means followed by different superscript letters differ significantly according to Tukey's HSD test following two-way ANOVA ($p < 0.05$). The cobalt nitrate precursor control produced no detectable growth inhibition against any tested fungal isolate at any tested concentration.

The cobalt nitrate precursor control was included as a synthesis-related control to evaluate the possible contribution of residual cobalt ions. This control showed no detectable antifungal inhibition against any of the tested fungal isolates under the applied experimental conditions and was not included in the statistical comparison with fungal treatments.

These findings demonstrate that conversion of *Spirogyra* sp. extract into cobalt oxide nanoparticles significantly enhanced antifungal activity compared with both the crude extract and cobalt nitrate precursor control. The absence of antifungal activity in the cobalt nitrate treatment suggests that free cobalt ions alone did not account for the observed inhibition under

the tested conditions. The enhanced activity of cobalt oxide nanoparticles may be associated with their nanoscale primary particle size, increased surface reactivity, and possible nanoparticle–cell interactions. Although ROS generation has been proposed as a possible mechanism for cobalt oxide nanoparticles in previous studies, this mechanism was not directly evaluated in the present study and requires further investigation [34, 35]. The differences in susceptibility among fungal isolates may be associated with variations in fungal cell wall composition, membrane permeability, antioxidant defense mechanisms, and physiological adaptation. Similar variability in antimicrobial responses has been reported among bacterial pathogens, where genetic determinants, virulence-associated factors, and adaptive mechanisms contribute to differences in microbial survival and resistance profiles [5, 36]. These findings support the concept that microbial responses to antimicrobial agents are influenced by the intrinsic biological characteristics of each microorganism. However, the specific mechanisms responsible for the different responses among fungal isolates in the present study were not investigated and require further evaluation. The lower sensitivity of *Fusarium solani* at 2500 µg/mL compared with other fungal isolates may reflect differences in fungal physiological characteristics and nanoparticle–cell interactions. Additionally, phytochemicals present in *Spirogyra* sp. extract, including phenolic compounds and flavonoids, may contribute to nanoparticle stabilization and may enhance antifungal activity through possible synergistic effects [4]. However, these proposed mechanisms require further experimental confirmation. The aggregation state of the synthesized cobalt oxide material should also be considered when interpreting its antifungal performance. Although the primary particles were within the nanoscale range, the formation of micron-sized aggregates may influence dispersion, effective surface area, and interaction with fungal cells. Therefore, the observed antifungal activity may result from the combined effects of primary particle characteristics and the aggregated morphology of the synthesized material. Overall, the antifungal activity of the synthesized cobalt oxide material appears to result from the combined influence of its physicochemical properties, aggregation behavior, and fungal biological variability rather than a single confirmed mechanism.

4. CONCLUSION

This study demonstrated the successful biosynthesis of cobalt oxide nanoparticles using the ethanolic extract of *Spirogyra* sp. Characterization analyses suggested the formation of crystalline cobalt oxide nanoparticles, while the synthesized nanoparticles exhibited enhanced in vitro antifungal activity compared with the crude algal extract. These findings indicate that *Spirogyra* sp. may serve as a potential biological resource for the green synthesis of cobalt oxide nanoparticles. However, the present results are preparation of cobalt oxide material was achieved using *Spirogyra* sp. extract. Further investigations are required to confirm the crystal phase, assess synthesis reproducibility, nanoparticle stability, cobalt ion release, cytotoxicity, ecotoxicity, environmental safety, and crop compatibility before considering any practical biomedical or agricultural applications.

ACKNOWLEDGMENTS

The authors would like to express their sincere gratitude to the Department of Biology, College of Science, Mustansiriyah University, Baghdad, Iraq, for providing the laboratory facilities necessary to conduct this study.

REFERENCES

[1] Nande, A., Raut, S., Michalska-Domanska, M., Dhoble, S.J. (2021). Green synthesis of nanomaterials using plant extract: A review. Current Pharmaceutical Biotechnology, 22(13): 1794-1811. https://doi.org/10.2174/1389201021666201117121452

[2] Paiva-Santos, A.C., Herdade, A.M., Guerra, C., et al. (2021). Plant-mediated green synthesis of metal-based nanoparticles for dermopharmaceutical and cosmetic applications. International Journal of Pharmaceutics, 597: 120311. https://doi.org/10.1016/j.ijpharm.2021.120311

[3] Sharma, D., Kanchi, S., Bisetty, K. (2015). Biogenic synthesis of nanoparticles: A review. Arabian Journal of Chemistry, 12(8): 3576-3600. https://doi.org/10.1016/j.arabjc.2015.11.002

[4] Raszewska-Famielec, M., Flieger, J. (2022). Nanoparticles for topical application in the treatment of skin dysfunctions—An overview of dermo-cosmetic and dermatological products. International Journal of Molecular Sciences, 23(24): 15980. https://doi.org/10.3390/ijms232415980

[5] Mohsin, A.S., Alsakini, A.H., Ali, M.R. (2022). Outbreak of drug resistance Escherichia coli phylogenetic F group associated urinary tract infection. Iranian Journal of Microbiology, 14(3): 341-350. https://doi.org/10.18502/ijm.v14i3.9771

[6] Mohsin, A.S., Ali, M.R., Alsakini, A.H. (2026). Biofilm-associated genes and their role in antibiotic resistance among clinical Staphylococcus aureus isolates. The Journal of Infection in Developing Countries, 20(3): 416-424. https://doi.org/10.3855/jidc.22026

[7] Leslie, J.F., Summerell, B.A., Bullock, S. (2006). The Fusarium Laboratory Manual. Ames, IA: Blackwell Pub.

[8] Azmir, J., Zaidul, I.S.M., Rahman, M.M., et al. (2013). Techniques for extraction of bioactive compounds from plant materials: A review. Journal of Food Engineering, 117(4): 426-436. https://doi.org/10.1016/j.jfoodeng.2013.01.014

[9] Politano, G.G. (2024). Optical properties of graphene nanoplatelets on amorphous germanium substrates. Molecules, 29(17): 4089. https://doi.org/10.3390/molecules29174089

[10] Tabassum, S., Saeed, M.A., Debnath, P., et al. (2026). Green-synthesized ZnO nano-crystallites as an electrochemical sensor for efficient detection of heavy metal. RSC Advances, 16(34): 32919-32931. https://doi.org/10.1039/d6ra01784c

[11] Simonnet, T., Grangeon, S., Claret, F., et al. (2024). Phase quantification using deep neural network processing of XRD patterns. IUCrJ, 11(5): 859-870. https://doi.org/10.1107/S2052252524006766

[12] Mourdikoudis, S., Pallares, R.M., Thanh, N.T.K. (2018). Characterization techniques for nanoparticles: Comparison and complementarity upon studying nanoparticle properties. Nanoscale, 10(27): 12871-

12934. https://doi.org/10.1039/c8nr02278j
[13] Besan, E.J., Fadel, M.N., Puteri, C.I.A., Munandar, D., Hartini, P.T. (2025). Green synthesis of silver nanoparticles using tamarind (Tamarindus indica) leaf extract and their application as an antibiofilm agent in pseudomonas aeruginosa infected wounds. Fundamental and Applied Research in Medicine and Allied Sciences Indonesia, 1(2): 45-55. https://doi.org/10.69855/farmasi.v1i2.434
[14] Sarwar, K., Nazli, Z.I.H., Munir, H., Aslam, M., Khalofah, A. (2025). Biosynthesis of zinc oxide nanoparticles using Moringa oleifera leaf extract, probing antibacterial and antioxidant activities. Scientific Reports, 15(1): 20413. https://doi.org/10.1038/s41598-025-08839-w
[15] Paul, C.A., Kumar, E.R., Abd El-Rehim, A.F., Yang, G. (2023). Cobalt oxide nanoparticles for biological applications: Synthesis and physicochemical characteristics for different natural fuels. Ceramics International, 49(24): 40244-40257. https://doi.org/10.1016/j.ceramint.2023.09.360
[16] Sheath, R.G., Wehr, J.D. (2015). Introduction to the freshwater algae. In Freshwater Algae of North America, pp. 1-11. https://doi.org/10.1016/B978-0-12-385876-4.00001-3
[17] Mahdi, Z.M., Al-Hussieny, A.A. (2022). Classification of some species algae in the Tigris River within the city of Baghdad-Iraq. Journal of Bionatura, 7(1): 72-79. https://doi.org/10.21931/RB/2022.07.03.53
[18] Guleria, S., Chawla, P., Relhan, A., Kumar, A., Bhasin, A., Zhou, J.L. (2024). Antibacterial and photocatalytic potential of bioactive compounds extracted from freshwater microalgae species (Spirogyra and Ocillatoria): A comparative analysis. Science of the Total Environment, 912: 169224. https://doi.org/10.1016/j.scitotenv.2023.169224
[19] Ali, R.H., Al-Maoula, M.S., Alwan, A.H. (2024). Effect of Cladophora glomerata extract against some fungal pathogens. Asian Journal of Water, Environment and Pollution, 21(6): 221-228. https://doi.org/10.3233/AJW240090
[20] Lage, V.M.G.B., Deegan, K.R., Sacramento, R.V., et al. (2024). Antifungal activity of microalgae in phytopathogenic fungi: A systematic review. Ciência e Natura, 46: e84584-e84584. https://doi.org/10.5902/2179460X84584
[21] Iravani, S. (2011). Green synthesis of metal nanoparticles using plants. Green Chemistry, 13(10): 2638-2650. https://doi.org/10.1039/c1gc15386b
[22] Abdallah, E.M., Alhudhaibi, A.M., Hussaini, I.M., Sulaiman, A.N. (2026). Harnessing biogenic nanoparticles for combating antibiotic resistance: Green synthesis, mechanistic insights, and biotechnological applications. Frontiers in Bioengineering and Biotechnology, 14: 1752199. https://doi.org/10.3389/fbioe.2026.1752199
[23] Ahmed, S., Ahmad, M., Swami, B.L., Ikram, S. (2016). Green synthesis of silver nanoparticles using Azadirachta indica aqueous leaf extract. Journal of Radiation Research and Applied Sciences, 9(1): 1-7. https://doi.org/10.1016/j.jrras.2015.06.006
[24] Saad, E.L., Salem, S.S., Fouda, A., Awad, M.A., El-Gamal, M.S., Abdo, A.M. (2018). New approach for antimicrobial activity and bio-control of various pathogens by biosynthesized copper nanoparticles using endophytic actinomycetes. Journal of Radiation Research and Applied Sciences, 11(3): 262-270. https://doi.org/10.1016/j.jrras.2018.05.003
[25] Samson, R.A., Houbraken, J., Thrane, U., Frisvad, J.C., Andersen, B. (2010). Food and indoor fungi Utrecht. The Netherlands: CBS 'KNAW'Fungal Biodiversity Centre.
[26] Fayyad, R.J., Dwaish, A.S., Sulman, I.M.A., Lefta, S.N. (2022). Phytochemical profiling of hot and cold alcoholic extract from Spirulina platensis alga and comparison between two extracts against multidrug-resistant bacteria. Research Journal of Pharmacy and Technology, 15(1): 399-404. http://doi.org/10.52711/0974-360X.2022.00066
[27] López-Miranda, J.L., Mares-Briones, F., Molina, G.A., et al. (2023). Sargassum natans I algae: An alternative for a greener approach for the synthesis of ZnO nanostructures with biological and environmental applications. Marine Drugs, 21(5): 297. https://doi.org/10.3390/md21050297
[28] Sharmila, G., Muthukumaran, C., Sandiya, K., et al. (2018). Biosynthesis, characterization, and antibacterial activity of zinc oxide nanoparticles derived from Bauhinia tomentosa leaf extract. Journal of Nanostructure in Chemistry, 8(3): 293-299. https://doi.org/10.1007/s40097-018-0271-8
[29] Jeon, Y.N., Ryu, S.J., Lee, H.Y., Kim, J.O., Baek, J.S. (2024). Green synthesis of silver nanoparticle using black mulberry and characterization, phytochemical, and bioactivity. Antibiotics, 13(8): 686. https://doi.org/10.3390/antibiotics13080686
[30] Zhang, Q., Gao, Y., Hu, J., He, T. (2025). Optical properties of chiral cobalt oxide nanoparticles. Inorganic Chemistry, 64(35): 17837-17843. https://doi.org/10.1021/acs.inorgchem.5c02646
[31] Jenkins, R., Snyder, R.L. (1996). Diffraction theory. In Introduction to X-ray Powder Diffractometry. https://doi.org/10.1002/9781118520994.ch3
[32] Patterson, A.L. (1939). The Scherrer formula for X-ray particle size determination. Physical Review, 56(10): 978. https://doi.org/10.1103/PhysRev.56.978
[33] Kumar, P., Thakur, N., Tapwal, A., Kumar, S. (2023). Enhancing the adsorption capacity of green/chemical synthesized hematite nanoparticles by copper doping: Removal of toxic Congo red dye and antioxidant activity. Applied Nanoscience, 13(9): 6591-6604. https://doi.org/10.1007/s13204-023-02943-x
[34] Diallo, A., Beye, A.C., Doyle, T.B., Park, E., Maaza, M. (2015). Green synthesis of Co3O4 nanoparticles via Aspalathus linearis: Physical properties. Green Chemistry Letters and Reviews, 8(3-4): 30-36. https://doi.org/10.1080/17518253.2015.1082646
[35] Bernardes, L.M.M., Malta, S.M., Santos, A.C.C., et al. (2025). Green synthesis, characterization, and antimicrobial activity of silver nanoparticles from water-soluble fractions of Brazilian Kefir. Scientific Reports, 15(1): 10626. https://doi.org/10.1038/s41598-025-95616-4
[36] Mohsin, A.S., Alsakini, A.H., Ali, M.R. (2022). Molecular characterization of Dr/Afa genes prevalent among multi drug resistant Escherichia coli isolated from urinary tract infections. Biomedicine, 42(3): 523-529. https://doi.org/10.51248/.v42i3.1632